

Analysis of radar allocation requirements for an IRST aided tracking of anti-ship missiles

Branko Ristic

DSTO
Blg 1082, PO Box 4331
Melbourne VIC 3001
Australia

branko.ristic@dsto.defence.gov.au

Alfonso Farina

SELEX Sistemi Integrati
Via Tiburtina Km 12.400
00131 Rome
Italy

afarina@selex-si.com

Marcel Hernandez

QinetiQ Ltd
St Andrew's Road
Malvern WR14 3PS
United Kingdom

marcel@signal.QinetiQ.com

Hwa-Tung Ong

DSTO
PO Box 1500
Edinburgh SA 5111
Australia

hwa-tung.ong@dsto.defence.gov.au

Abstract - *The paper presents an analysis of the phased array radar allocation demands, when tracking highly manoeuvrable anti-ship missiles (ASM) using a collocated radar/IRST sensor combination. The motion of the ASM is modelled using the quantized acceleration levels. The principal aim of this analysis is to determine an upper bound on the average radar update time. This bound follows from a Cramér-Rao type error bound for the estimation of linear jump Markov dynamic systems [1]. Given a dynamic motion model of an ASM, the IRST/radar sensor characteristics and a tolerable level of target state estimation error, we can theoretically predict the maximum average update time required for the phased-array radar. The presented analysis allows us to quantify the IRST benefits in ASM defence, without a need for extensive Monte Carlo simulations.*

Keywords: Tracking, performance bound, resource allocation, anti-ship missile defence, IRST, phased-array radar, data fusion.

1 Introduction

Modern anti-ship missiles (e.g. sea-skimmers, BUNT missiles, anti-radiation missiles) combine low-altitude flight, low radar-cross-section, high speed and maneuverability, and as such represent a serious threat beyond the capabilities of a radar-only surveillance system. In an attempt to overcome this limitation, a modern shipboard surveillance system would typically complement a phased array radar with a passive infra-red search and track (IRST) sensor [2, 3]. Some of the characteristics of a generic IRST sensor are: it is a passive sensor thus it cannot in principle be detected and, consequently, jammed; it provides angular mea-

surements (azimuth and elevation) of target position; it is not affected by multipath at low elevation angles; it has a very high angular accuracy and resolution wrt radar; its detection range against anti-ship missiles is speed dependent (longer range for higher speed) and consequently provides a relatively constant “time to closest point of approach”.

The principle of operation of an IRST aided radar surveillance is as follows: the IRST passively scans the horizon at a constant scanning interval in order to detect low altitude threats. Each such detection serves as an *alert* that is then used to allocate and cue an agile beam confirm dwell with a pulse-Doppler waveform of much higher energy than the normal radar surveillance waveform. This principle of IRST aided phased-array radar operation leads to a significant increase in the confirmation range and a substantial decrease in the radar resources required for track maintenance. As a consequence, more tracks can be maintained and more radar resources can be applied to track initiation [4, Sec.14.9].

The paper explores the theoretical bound on phased array radar allocation when tracking highly manoeuvrable anti-ship missiles (ASM) using a collocated radar/IRST sensor combination. The assumption is that during the ASM tracking, the phased array is requested (to allocate a beam along a certain direction, transmit a suitable waveform, and process the received echo) whenever the track error exceeds a certain threshold. The motion of the ASM is modelled using the quantized acceleration levels in three-dimensions. The principal tool in developing the bound on radar allocation is a Cramér-Rao type error bound for the estimation of linear jump Markov dynamic systems [1]. Thus given a dynamic motion model of an ASM, the IRST/radar sensor characteristics and a tolerable level of target state estimation error, we can theoretically predict the maximum average update time required for

Report Documentation Page

*Form Approved
OMB No. 0704-0188*

Public reporting burden for the collection of information is estimated to average 1 hour per response, including the time for reviewing instructions, searching existing data sources, gathering and maintaining the data needed, and completing and reviewing the collection of information. Send comments regarding this burden estimate or any other aspect of this collection of information, including suggestions for reducing this burden, to Washington Headquarters Services, Directorate for Information Operations and Reports, 1215 Jefferson Davis Highway, Suite 1204, Arlington VA 22202-4302. Respondents should be aware that notwithstanding any other provision of law, no person shall be subject to a penalty for failing to comply with a collection of information if it does not display a currently valid OMB control number.

1. REPORT DATE JUL 2006	2. REPORT TYPE	3. DATES COVERED 00-00-2006 to 00-00-2006			
4. TITLE AND SUBTITLE Analysis of radar allocation requirements for an IRST aided tracking of anti-ship missiles		5a. CONTRACT NUMBER			
		5b. GRANT NUMBER			
		5c. PROGRAM ELEMENT NUMBER			
6. AUTHOR(S)		5d. PROJECT NUMBER			
		5e. TASK NUMBER			
		5f. WORK UNIT NUMBER			
7. PERFORMING ORGANIZATION NAME(S) AND ADDRESS(ES) DSTO,Bldg 1082, PO Box 4331,Melbourne VIC 3001,Australia,		8. PERFORMING ORGANIZATION REPORT NUMBER			
9. SPONSORING/MONITORING AGENCY NAME(S) AND ADDRESS(ES)		10. SPONSOR/MONITOR'S ACRONYM(S)			
		11. SPONSOR/MONITOR'S REPORT NUMBER(S)			
12. DISTRIBUTION/AVAILABILITY STATEMENT Approved for public release; distribution unlimited					
13. SUPPLEMENTARY NOTES 9th International Conference on Information Fusion, 10-13 July 2006, Florence, Italy. Sponsored by the International Society of Information Fusion (ISIF), Aerospace & Electronic Systems Society (AES), IEEE, ONR, ONR Global, Selex - Sistemi Integrati, Finmeccanica, BAE Systems, TNO, AFOSR's European Office of Aerospace Research and Development, and the NATO Undersea Research Centre. U.S. Government or Federal Rights License					
14. ABSTRACT see report					
15. SUBJECT TERMS					
16. SECURITY CLASSIFICATION OF:			17. LIMITATION OF ABSTRACT	18. NUMBER OF PAGES	19a. NAME OF RESPONSIBLE PERSON
a. REPORT unclassified	b. ABSTRACT unclassified	c. THIS PAGE unclassified	Same as Report (SAR)	8	

the phased-array radar (which translates into the required energy per unit time). The significance of this is that one can predict, even before the system is built, the upper limit on the capability of the IRST/radar surveillance system. In addition, the relative merits of having an IRST sensor to aid in tracking can then be easily quantified, without a need for extensive Monte Carlo simulations. The model of the phased array radar that we consider in this study is somewhat simplified because it ignores the details concerning the radiated waveform, the signal processing and the multifunctional capability of radar (i.e. the interleaving of functions such as search, track, etc). However, the main ideas presented here can be directly extended to more detailed sensor models.

The paper is organised as follows. Section 2 presents a mathematical formulation of the problem, with details of the ASM motion model and sensor measurement models. Section 3 is devoted to the theoretical bound for radar allocation. Numerical analysis is presented in Section 4 and the conclusions of the study are drawn in Section 5.

2 Problem formulation

We consider shipboard collocated phased-array radar and an IRST, targeted by a highly manoeuvrable ASM (see Fig.1). The two sensors are assumed to be perfectly registered. The target (ASM) state is $\mathbf{x} = [x \ \dot{x} \ y \ \dot{y} \ z \ \dot{z}]^T$. The motion model that we adopt for a generic ASM is described next.

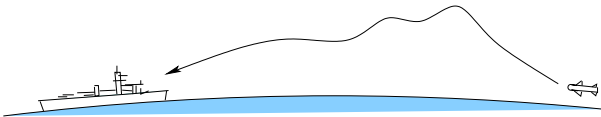


Figure 1: Illustration of the engagement scenario

2.1 Dynamic motion models

Various target dynamics models applicable to anti-ship missile motion (both subsonic and supersonic) have been proposed in the literature, such as the nearly constant velocity model, constant acceleration model, coordinated turn model, Singer (coloured process noise) model, “weave” manoeuvre model, “BUNT” manoeuvre model, to name a few [5, 6, 7]. Since this plethora of (both linear and non-linear) models is neither exclusive nor exhaustive, we adopt an alternative modelling approach based on quantized acceleration levels [8, 9]. The assumption here is that the acceleration is piece-wise constant and its mean is taken from a finite set of acceleration levels. The perturbations upon this constant acceleration is modelled as white Gaussian noise. Switching from one acceleration level to another is modelled by a first-order Markov chain.

The adopted target dynamic model is expressed as:

$$\mathbf{x}_{k+1} = \mathbf{A}_k \mathbf{x}_k + \mathbf{B}_k \mathbf{a}(\mathbf{r}_{k+1}) + \mathbf{w}_k \quad (1)$$

where k is the index assigned to the continuous-time instant t_k ,

$$\mathbf{A}_k = \mathbf{I}_3 \otimes \begin{bmatrix} 1 & T_k \\ 0 & 1 \end{bmatrix} \quad (2)$$

$$\mathbf{B}_k = \begin{bmatrix} T_k^2/2 & 0 & 0 \\ T_k & 0 & 0 \\ 0 & T_k^2/2 & 0 \\ 0 & T_k & 0 \\ 0 & 0 & T_k/2 \\ 0 & 0 & T_k \end{bmatrix}. \quad (3)$$

Here \mathbf{I}_n denotes an $n \times n$ identity matrix, \otimes is the Kronecker product, $T_k = t_{k+1} - t_k$ is the sampling interval; \mathbf{w}_k is a 6×1 vector of zero-mean white Gaussian noise with nonsingular covariance matrix

$$\mathbf{Q}_k = q \cdot \text{block-diag}(\Theta_k, \Theta_k, \Theta_k) \quad (4)$$

where q is a parameter related to process noise intensity [7, p.270], and

$$\Theta_k = \begin{bmatrix} T_k^3/3 & T_k^2/2 \\ T_k^2/2 & T_k \end{bmatrix}. \quad (5)$$

The acceleration vector $\mathbf{a}(\mathbf{r}_{k+1})$ in (1) is a function of a discrete-valued 3D random vector $\mathbf{r}_{k+1} = [r_x \ r_y \ r_z]^T$ which determines the regime (i.e. acceleration level) of target motion during the period $t_k < t \leq t_{k+1}$. Here $r_x \in \mathcal{R}_x$, $r_y \in \mathcal{R}_y$, $r_z \in \mathcal{R}_z$ with

$$\begin{aligned} \mathcal{R}_x &= \{-s_x, -s_x + 1, \dots, -1, 0, 1, \dots, s_x - 1, s_x\} \\ \mathcal{R}_y &= \{-s_y, -s_y + 1, \dots, -1, 0, 1, \dots, s_y - 1, s_y\} \\ \mathcal{R}_z &= \{-s_z, -s_z + 1, \dots, -1, 0, 1, \dots, s_z - 1, s_z\} \end{aligned}$$

with s_x , s_y , and s_z being positive integers. The acceleration vector is then

$$\mathbf{a}(\mathbf{r}_{k+1}) = [a_0 r_x \ b_0 r_y \ c_0 r_z]^T \quad (6)$$

where a_0 , b_0 and c_0 are suitably chosen acceleration quantum values (or units) along x , y and z axes, respectively. The acceleration is thus discretised into $S = (2s_x + 1)(2s_y + 1)(2s_z + 1)$ possible levels. The target motion regime \mathbf{r}_k can switch between S models in a random manner. The evolution of the motion regime is modelled by a first-order time-homogeneous Markov chain with known:

1. transitional probabilities

$$\pi_{\mathbf{i}, \mathbf{j}} \triangleq \mathbb{P}\{\mathbf{r}_{k+1} = \mathbf{j} | \mathbf{r}_k = \mathbf{i}\}. \quad (7)$$

where $\mathbf{i} = [i_x \ i_y \ i_z]^T$, $\mathbf{j} = [j_x \ j_y \ j_z]^T$, with $i_x, j_x \in \mathcal{R}_x$, $i_y, j_y \in \mathcal{R}_y$, $i_z, j_z \in \mathcal{R}_z$; the transitional probability matrix $[\pi_{\mathbf{i}, \mathbf{j}}]$ is a square $S \times S$ matrix.

2. initial regime probabilities $p_1(\mathbf{i}) \triangleq \mathbb{P}(\mathbf{r}_1 = \mathbf{i})$, where $\mathbf{i} = [i_x \ i_y \ i_z]^T$, and $i_x \in \mathcal{R}_x$, $i_y \in \mathcal{R}_y$, $i_z \in \mathcal{R}_z$.

The transitional and initial regime probabilities are non-negative and normalised, that is:

$$\sum_{\mathbf{i}} p_1(\mathbf{i}) = 1, \quad \sum_{\mathbf{j}} \pi_{\mathbf{i}, \mathbf{j}} = 1. \quad (8)$$

2.2 Measurement models

The IRST provides target azimuth and elevation measurements at regular sampling intervals T . The location of the IRST/radar in the local Cartesian coordinates is given by vector $(x_o, y_o, z_o)^T$, however, in order to simplify notation we will assume that $x_o = y_o = z_o = 0$. The IRST measurement vector at time k , $\mathbf{z}_k^I = [\theta_k^I \ \epsilon_k^I]^T$ is then given by

$$\mathbf{z}_k^I = \mathbf{h}_k^I(\mathbf{x}_k) + \mathbf{v}_k^I \quad (9)$$

where

$$\mathbf{h}_k^I(\mathbf{x}_k) = \begin{pmatrix} \arctan \frac{y_k}{x_k} \\ \arcsin \frac{z_k}{\sqrt{x_k^2 + y_k^2 + z_k^2}} \end{pmatrix} \quad (10)$$

and \mathbf{v}_k^I is the IRST measurement noise, assumed to be zero-mean Gaussian with covariance matrix $\mathbf{R}^I = \text{diag}(\sigma_{\theta,I}^2, \sigma_{\epsilon,I}^2)$.

The phased-array radar is requested to provide measurements of target range, range-rate, azimuth and elevation based on the adopted radar allocation strategy. The radar measurement vector at time k , $\mathbf{z}_k^R = [\rho_k^R \ \dot{\rho}_k^R \ \theta_k^R \ \epsilon_k^R]^T$ is given by

$$\mathbf{z}_k^R = \mathbf{h}_k^R(\mathbf{x}_k) + \mathbf{v}_k^R \quad (11)$$

where

$$\mathbf{h}_k^R(\mathbf{x}_k) = \begin{pmatrix} \frac{\sqrt{x_k^2 + y_k^2 + z_k^2}}{x_k \dot{x}_k + y_k \dot{y}_k + z_k \dot{z}_k} \\ \arctan \frac{y_k}{x_k} \\ \arcsin \frac{z_k}{\sqrt{x_k^2 + y_k^2 + z_k^2}} \end{pmatrix} \quad (12)$$

and \mathbf{v}_k^R is the radar measurement noise, assumed to be zero-mean Gaussian with covariance matrix $\mathbf{R}^R = \text{diag}(\sigma_{\rho}^2, \sigma_{\dot{\rho}}^2, \sigma_{\theta,R}^2, \sigma_{\epsilon,R}^2)$.

In this analysis we will assume that the radar allocation is requested whenever the target track error (in position, range, elevation or azimuth) exceed a predefined threshold.

3 Radar allocation bound

The key idea of this paper is to compute the theoretical bound on required radar allocation using the posterior Cramér-Rao lower bound (PCRLB) for target state estimation. Namely, if $\hat{\mathbf{x}}_k$ is an unbiased target state estimator with covariance \mathbf{C}_k , then the following inequality holds:

$$\mathbf{C}_k \triangleq \mathbb{E}[(\mathbf{x}_k - \hat{\mathbf{x}}_k)(\mathbf{x}_k - \hat{\mathbf{x}}_k)^T] \geq \mathbf{P}_k \quad (13)$$

where \mathbf{P}_k is the PCRLB and its inverse $\mathbf{J}_k = \mathbf{P}_k^{-1}$ is the Fisher information matrix (FIM) defined in [10]. Substantial advances have recently been reported in development of the PCRLB for target tracking, such as an efficient PCRLB computation in the context of nonlinear filtering [11] and the PCRLBs when measurements are of uncertain origin [12, 13, 14, 15, 16]. In this paper we will use the best-fitted Gaussian (BFG) approximation to the PCRLB for Markovian switching systems [1] because of the dynamic model of the ASM described in Sec.2.1.

3.1 The BFG approximation for jump Markov linear systems

In order to compute the PCRLB for the dynamic model described in Sec.2.1, we have to augment the state vector to include units a_0 , b_0 and c_0 . We point out that these units are known, hence not required to be estimated; this fact will be reflected in the initial covariance matrix and the process noise covariance. We augment the state vector as follows [17]:

$$\tilde{\mathbf{x}}_k = [x \ \dot{x} \ a_0 \ y \ \dot{y} \ b_0 \ z \ \dot{z} \ c_0]^T \quad (14)$$

so that the dynamic equation (1) can be written as:

$$\tilde{\mathbf{x}}_{k+1} = \mathbf{F}_k^{\Gamma_{k+1}} \tilde{\mathbf{x}}_k + \tilde{\mathbf{w}}_k \quad (15)$$

where

$$\mathbf{F}_k^{\Gamma_{k+1}} = \mathbf{I}_3 \otimes \begin{bmatrix} 1 & T_k & \frac{T_k^2}{2} \cdot r_{\psi,k+1} \\ 0 & 1 & T_k \cdot r_{\psi,k+1} \\ 0 & 0 & 1 \end{bmatrix}. \quad (16)$$

Here ψ takes values x , y and z (in this order). The process noise $\tilde{\mathbf{w}}_k$ is again zero-mean Gaussian, with covariance matrix $\tilde{\mathbf{Q}}_k = q \cdot \text{block-diag}(\tilde{\Theta}_k, \tilde{\Theta}_k, \tilde{\Theta}_k)$, where $\tilde{\Theta}_k = \text{diag}(\Theta_k, 0)$.

When the dynamic equation is given in the form of (15), we can apply the best-fitted Gaussian approximation to compute the PCRLB [1]. The BFG-PCRLB computation requires us to specify the initial target state $\tilde{\mathbf{x}}_o$ and its covariance matrix, $\tilde{\mathbf{P}}_o$, the initial regime probabilities $p_1(i)$, the transitional probabilities $\pi_{i,j}$, process noise covariance and sensor characteristics (measurement error standard deviations and the sampling time).

The main idea of the BFG-PCRLB approximation is to approximate the linear jump Markov system described by (15) with the linear non-switching system

$$\tilde{\mathbf{x}}_{k+1} \approx \Phi_k \tilde{\mathbf{x}}_k + \mathbf{u}_k \quad (17)$$

where \mathbf{u}_k is an “equivalent” zero-mean white Gaussian random vector with a covariance matrix Σ_k . A straightforward procedure for the sequential computation of Φ_k and Σ_k ensures that the first and the second moment of models (15) and (17) are identical [1]. This procedure is given in Table 1.

Example 1. Consider the case where a ship is located in 3D space at $(0,0,0)m$ and the initial location of the ASM is $(17321, 10000, 0)m$. The ASM is heading towards the ship with the speed of 400m/s. The initial covariance matrix is $\tilde{\mathbf{P}}_o = \text{diag}(\sigma_x^2, \sigma_v^2, \delta, \sigma_y^2, \sigma_v^2, \delta, \sigma_z^2, \sigma_v^2, \delta)$, where $\sigma_x = 21$ m, $\sigma_y = 13.5$ m and $\sigma_z = 12.8$ m (computed using the first (IRST, radar) associated measurement pair and the spherical-to-Cartesian conversion). Furthermore, $\sigma_v = 10$ m/s, and $\delta \ll 1$ is a very small value which reflects the fact that the quantum values a_0, b_0, c_0 are known (δ has to be non-zero so that $\tilde{\mathbf{P}}_o$ is non-singular).

The transitional probabilities are set as follows: the non-switching probability is $\pi_{i,i} = \alpha$ and the remaining

Table 1: The BFG computation of Φ_k and Σ_k

Initialisation: $\epsilon = \tilde{\mathbf{x}}_o$, $\mathcal{C} = \tilde{\mathbf{P}}_o$.

For $k = 1, 2, 3, \dots$

$$\begin{aligned}\Phi_{k-1} &= \sum_{\mathbf{i}} \mathbf{F}_{k-1}^{\mathbf{i}} p_k(\mathbf{i}) \\ \mathcal{C}_k &= \sum_{\mathbf{i}} p_k(\mathbf{i}) [\mathbf{F}_{k-1}^{\mathbf{i}} (\mathcal{C}_{k-1} + \epsilon_{k-1} \epsilon_{k-1}^T) (\mathbf{F}_{k-1}^{\mathbf{i}})^T \\ &\quad + \tilde{\mathbf{Q}}_{k-1}] - \Phi_{k-1} \epsilon_{k-1} \epsilon_{k-1}^T \Phi_{k-1}^T \\ \Sigma_{k-1} &= \mathcal{C}_k - \Phi_{k-1} \mathcal{C}_{k-1} \Phi_{k-1} \\ \epsilon_k &= \Phi_{k-1} \epsilon_{k-1} \\ p_{k+1}(\mathbf{i}) &= \sum_{\mathbf{j}} \pi_{\mathbf{j}, \mathbf{i}} p_k(\mathbf{j})\end{aligned}$$

End

$1 - \alpha$ is equally distributed among the switching cases so that normalisation in (8) holds. The initial non-accelerating regime probability is set to 1, i.e. $\mathbb{P}(r_{x,1} = 0, r_{y,1} = 0, r_{z,1} = 0) = 1$. The units of acceleration are $a_0 = b_0 = c_0 = 1g$, where $g = 9.81\text{m/s}^2$. Figure 2 shows the 2σ uncertainty ellipsoids in the $X - Y$ plane of the BFG approximation for $\alpha = 0.9$ and $q = 0.001 \text{ m}^2/\text{s}^3$ at time steps $t_k = kT_k$, with $T_k = 0.5\text{s}$, $k = 0, 1, \dots$. In red we show the results for $s_x = s_y = 4$ and in blue for $s_x = s_y = 8$ (in both cases $s_z = 0$).

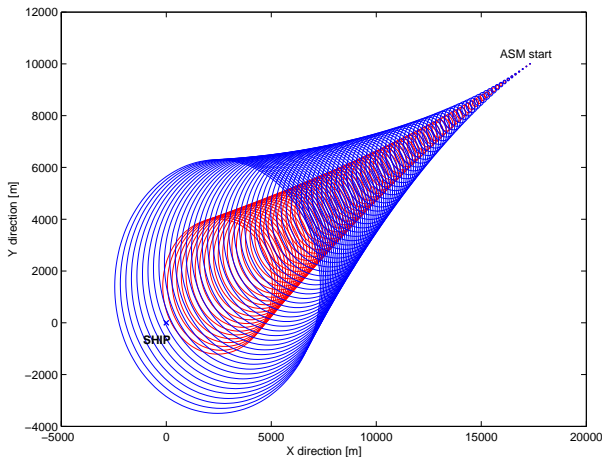


Figure 2: Uncertainty ellipsoids of the BFG approximation for different levels of quantized acceleration. In red is the case $\mathcal{R}_x = \mathcal{R}_y = \{-4g, -3g, \dots, 0, \dots, 3g, 4g\}$, in blue is $\mathcal{R}_x = \mathcal{R}_y = \{-8g, -7g, \dots, 0, \dots, 7g, 8g\}$.

The first observation from Figure 2 is that the mean of the BFG approximation is directed towards its aim (the ship), despite the fact that the ASM is manoeuvring. This is true whenever the transitional probability matrix is symmetric and the acceleration space is quantized symmetrically around the zero acceleration in all directions. The second more obvious observation

is that the uncertainty grows with the larger span between the minimum and maximum acceleration levels (in this case red corresponds to $\pm 4g$ while blue corresponds to $\pm 8g$). The value of α also influences the size of the uncertainty ellipsoid (results not shown here): the higher the value of α , the smaller the uncertainty.

3.2 FIM measurement contribution

Once we determine Φ_k and Σ_k , we can apply the Riccati-type recursion to compute the FIM [11]:

$$\mathbf{J}_k = \mathbf{J}_p(k) + \mathbf{J}_z(k) \quad (k = 1, 2, \dots) \quad (18)$$

where matrix

$$\mathbf{J}_p(k) = (\Phi_{k-1} \mathbf{J}_{k-1}^{-1} \Phi_{k-1}^T + \Sigma_{k-1})^{-1} \quad (19)$$

is the *predicted FIM* and matrix $\mathbf{J}_z(k)$ is the *measurement contribution* to the FIM.

The FIM measurement contribution $J_z(k)$ in general depends on sensor measurement functions (in our case \mathbf{h}_k^I and \mathbf{h}_k^R), target trajectory, and the detection characteristics of sensors (the probability of detection P_d and the probability of false alarm P_{fa}). The non-ideal detection characteristics of sensors ($P_d \leq 1$ and $P_{fa} \geq 0$) introduce uncertainty in the measurement origin, which reflects itself in a reduction of the measurement contribution to the FIM. A comprehensive analysis of the influence of $P_d \leq 1$ and $P_{fa} \geq 0$ on $J_z(k)$ is presented in [16]. For simplicity, however, in this study we assume zero false alarms rates, while the effect of $P_d \leq 1$ will be taken into account as follows:

$$\mathbf{J}_z(k) = P_d \cdot \mathbb{E} \{ \mathbf{H}_k^T \mathbf{R}_k^{-1} \mathbf{H}_k \}. \quad (20)$$

The resulting bound, referred to as the information reduction factor PCRLB [15], is a conservative but reasonable approximation, which becomes fairly accurate after a few initial scans. The term \mathbb{E} in (20) is the expectation operator and \mathbf{H}_k is the Jacobian of measurement function \mathbf{h}_k :

$$\mathbf{H}_k(\tilde{\mathbf{x}}_k) = [\nabla_{\tilde{\mathbf{x}}_k} \mathbf{h}_k^T(\tilde{\mathbf{x}}_k)]^T \quad (21)$$

evaluated at the true value of the $\tilde{\mathbf{x}}_k$. Depending on the source of a measurement at time k (IRST or radar), function \mathbf{h}_k takes the form of \mathbf{h}_k^I or \mathbf{h}_k^R , respectively. Matrix \mathbf{R}_k in (20) is the measurement covariance, and takes the form of \mathbf{R}_k^I or \mathbf{R}_k^R , depending on the source of the measurement. Similarly, P_d is the probability of detection of a sensor (P_d^I for IRST; P_d^R for radar), and typically is a function of target range. If at time k , both radar and IRST measurements are requested, due to their mutual independence, eq.(20) takes an additive form:

$$\begin{aligned}\mathbf{J}_z(k) &= P_d^R \mathbb{E} \{ (\mathbf{H}_k^R)^T (\mathbf{R}_k^R)^{-1} \mathbf{H}_k^R \} \\ &\quad + P_d^I \mathbb{E} \{ (\mathbf{H}_k^I)^T (\mathbf{R}_k^I)^{-1} \mathbf{H}_k^I \}.\end{aligned}$$

Jacobian \mathbf{H}_k^R is a 4×9 matrix; Jacobian \mathbf{H}_k^I has the same entries as the lower 2×9 submatrix of \mathbf{H}_k^R . Hence we present only the elements of \mathbf{H}_k^R , which are easily

obtained by differentiation. The non-zero elements of \mathbf{H}_k^R are as follows:

$$\begin{aligned}
\mathbf{H}_k^R[1, 1] &= \mathbf{H}_k^R[2, 2] = \frac{x_k}{\rho_k} \\
\mathbf{H}_k^R[1, 4] &= \mathbf{H}_k^R[2, 5] = \frac{y_k}{\rho_k} \\
\mathbf{H}_k^R[1, 7] &= \mathbf{H}_k^R[2, 8] = \frac{z_k}{\rho_k} \\
\mathbf{H}_k^R[2, 1] &= \frac{\dot{x}_k(y_k^2 + z_k^2) - x_k(y_k\dot{y}_k + z_k\dot{z}_k)}{\rho_k^3} \\
\mathbf{H}_k^R[2, 4] &= \frac{\dot{y}_k(x_k^2 + z_k^2) - y_k(x_k\dot{x}_k + z_k\dot{z}_k)}{\rho_k^3} \\
\mathbf{H}_k^R[2, 7] &= \frac{\dot{z}_k(x_k^2 + y_k^2) - z_k(x_k\dot{x}_k + y_k\dot{y}_k)}{\rho_k^3} \\
\mathbf{H}_k^R[3, 1] &= -\frac{y_k}{x_k^2 + y_k^2}, \quad \mathbf{H}_k^R[3, 4] = \frac{x_k}{x_k^2 + y_k^2} \\
\mathbf{H}_k^R[4, 1] &= -\frac{x_k z_k}{\rho_k^2 \sqrt{x_k^2 + y_k^2}} \\
\mathbf{H}_k^R[4, 4] &= -\frac{y_k z_k}{\rho_k^2 \sqrt{x_k^2 + y_k^2}} \\
\mathbf{H}_k^R[4, 1] &= \frac{\sqrt{x_k^2 + y_k^2}}{\rho_k^2}
\end{aligned}$$

where $\rho_k = \sqrt{x_k^2 + y_k^2 + z_k^2}$.

In order to compute the measurement contribution to the FIM as in (20), we would need to average the product $\mathbf{H}_k^T \mathbf{R}_k^{-1} \mathbf{H}_k$ over all possible realisations of the state vector \mathbf{x}_k . In general this can be done numerically, e.g. via a sample based technique [1]. In our analysis, however, we will consider one particular ASM trajectory (see Sec.4.1) for which we will compute the measurement contribution to the FIM.

3.3 Radar allocation requirement

The IRST provides its measurements at a regular sampling interval T_i . The phased-array radar measurement is required for track update whenever the predicted RMS error in estimating the position of the ASM exceeds a certain threshold η . The radar allocation test is carried out every $T_k < T_i$ seconds and formally states: allocate radar if

$$\text{RMSE}_{pos}^{pred} \approx \sqrt{\mathbf{J}_p^{-1}[1, 1] + \mathbf{J}_p^{-1}[4, 4] + \mathbf{J}_p^{-1}[7, 7]} \geq \eta, \quad (22)$$

where \mathbf{J}_p is the predicted FIM of (19). The exact expression for the RMS error in the predicted position would involve the cross-terms such as $\mathbf{J}_p[1, 4]$, $\mathbf{J}_p[1, 7]$, etc. (see [10, p. 9] for the general formulation of the PCRLB for the nonlinear transformation of the state vector). For discussion on other rules for radar allocation see [4, Sec.14.4].

4 Numerical analysis

4.1 Simulation setup

The simulated missile trajectory corresponds to a supersonic ASM which performs a weaving manoeuvre.

The initial speed is 700 m/s, with acceleration load in the horizontal plane oscillating with a period of 5 seconds. The height of the missile is constant at 10 m. The trajectory is shown in Figure 3 (top-down view) for peak acceleration loads of 4, 8, 12 and 16 g.

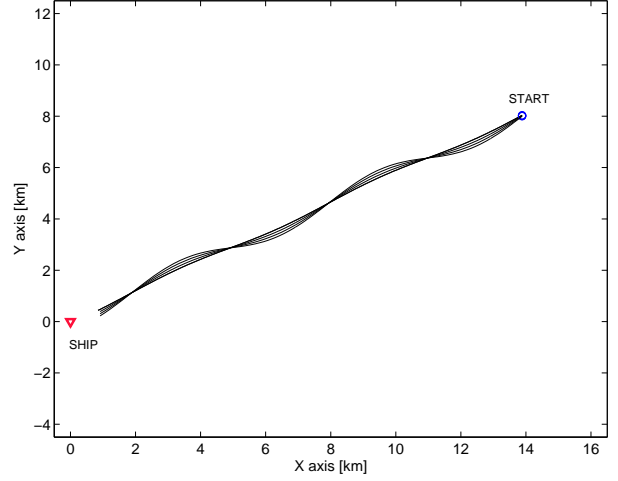


Figure 3: Test missile trajectory (with varying levels of acceleration loads)

Numerical analysis is carried out assuming that the radar has confirmed the initial IRST alert and that the track on the incoming ASM has been established by fusing the initial radar and IRST measurements. The elements of the radar measurement covariance matrix \mathbf{R}_k^R are specified as: $\sigma_\rho = 30$ m, $\sigma_{\dot{\rho}} = 3$ m/s, $\sigma_{\theta, R} = 3.0$ mrad and $\sigma_{\epsilon, R} = 4.5$ mrad. The accuracy of IRST measurements is characterised by $\sigma_{\theta, I} = 0.25$ mrad and $\sigma_{\epsilon, I} = 0.64$ mrad. The range at which missile tracking starts is 16 km. The initial covariance matrix is for the case of IRST/radar combination specified by $\hat{\mathbf{P}}_o = \text{diag}(\sigma_x^2, \sigma_v^2, \delta, \sigma_y^2, \sigma_v^2, \delta, \sigma_z^2, \sigma_v^2, \delta)$, where $\sigma_x = 21.8$ m, $\sigma_y = 13.4$ m and $\sigma_z = 12.8$ m, $\sigma_v = 10$ m/s and $\delta = 10^{-8}$. For comparison, we also consider the radar-only (no IRST) case, with $\sigma_x = 39$ m, $\sigma_y = 53$ m and $\sigma_z = 75$ m (these values were obtained by spherical-to-Cartesian conversion).

The probability of detection P_d for both sensors is modelled next. In the case of the IRST, following the description in [4, Sec.2.3], the P_d versus range curve is shown in Fig.4 in red solid line. This curve is obtained assuming $P_d = 0.9$ at the nominal range of 17 km. For the case of a radar, an attempt has been made to incorporate the effect of specular multipath on P_d , as shown in Fig.4 in blue thin line. The values of multipath nulls for the radar cannot be known in advance as they depend on the height of the missile. In general multipath also deteriorates the accuracy of elevation angle radar measurements [18], although this effect has not been included in the model.

4.2 Numerical results

First we analyze the positional RMS error as a function of time for: (1) the case where an IRST is available to complement the phased-array radar in tracking an ASM; the IRST is scanning the horizon with $T_i = 1$ s;

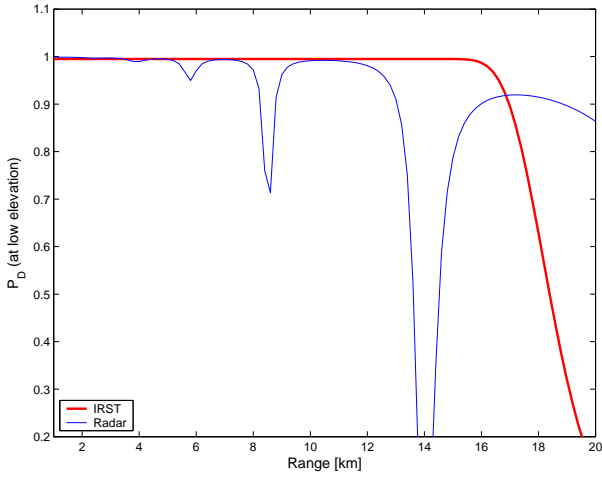


Figure 4: Probability of detection versus range (P_d^I in red; P_d^R in blue)

(2) the radar-only tracking case. The results are shown in Fig.5 for $s_x = s_y = 4$, $s_z = 0$, $a_0 = b_0 = c_0 = 1g$, $T_k = 0.2$ s, $\alpha = 0.9$, $q = 0.0001$ and $\eta = 100$ m.

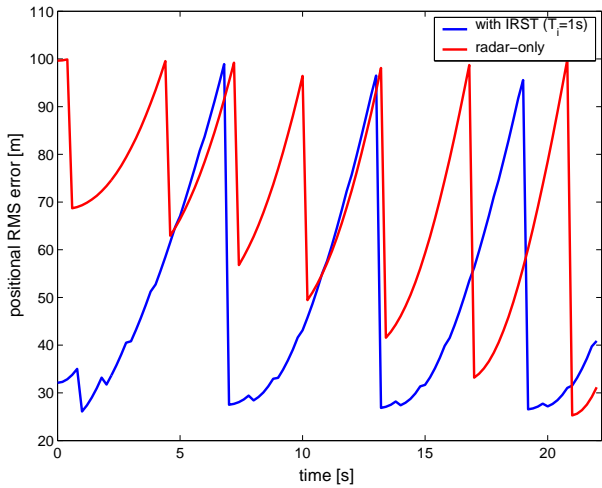
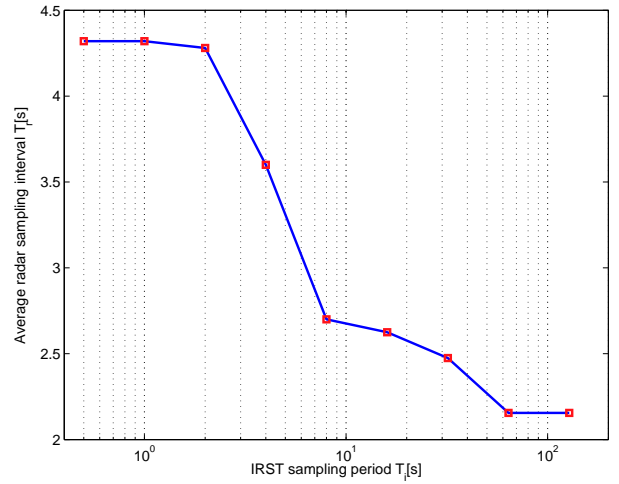


Figure 5: Positional RMS error with IRST (blue) and without an IRST (red)

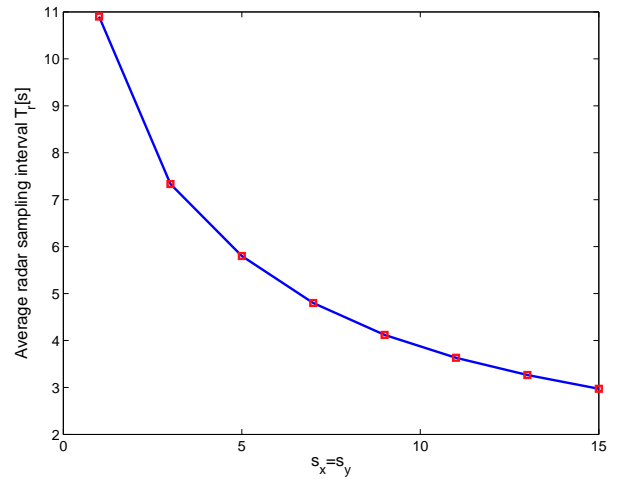
From Fig.5 we note that sharp drops in the RMS error indicate the instances when a radar allocation was requested. Thus, if the radar is operating alone, it is requested to revisit the target 7 times; with addition of the IRST, however, the radar is requested only 3 times.

Next, in Fig.6, we analyse the average update time of the phased-array radar as a function of: (a) the sampling period of IRST T_i and (2) the value of $s_x = s_y$ which corresponds to manoeuvre ability of the incoming missile. In preparation of this figure we used the same trajectory and parameters as indicated above, unless otherwise stated.

Fig.6.(a) was obtained for $s_x = s_y = 8$. Observe that the IRST sampling intervals (T_i) of 0.5, 1 and 2 seconds, result in very similar radar allocation requirements. There is a dramatic drop in average T_r (i.e. a growing demand for the radar) when T_i is increased from 2 seconds to 8 seconds; finally, for $T_i \geq 64$



(a)



(b)

Figure 6: Average radar update time (in seconds) versus: (a) the IRST sampling period T_i ; (b) the manoeuvre ability of the missile in the horizontal plane ($s_x = s_y$)

seconds, the IRST becomes irrelevant and the system performs as if the radar is alone.

Fig.6.(b) was obtained for $s_z = 0$ and $T_i = 1$ s. Observe that the higher the manoeuvre ability of the missile, the smaller the average update time of the radar (i.e. the greater demand for the radar).

4.3 Comparison with an EKF

Next we compare the theoretical bound on average radar sampling interval T_r , with the update time of an Extended Kalman filter (EKF), designed to process both radar and IRST measurements using the appropriate measurement functions \mathbf{h}_k^R and \mathbf{h}_k^I . The EKF assumed a constant velocity dynamic motion model, with a large amount of white process noise to account for ASM manoeuvres. The radar allocation test is carried out as in (22), except that \mathbf{J}_p^{-1} is replaced by the EKF predicted covariance. The radar update times of the EKF were averaged over 10 Monte Carlo runs and plotted against the IRST sampling period in Fig.7.

Over the range of IRST sampling periods examined,

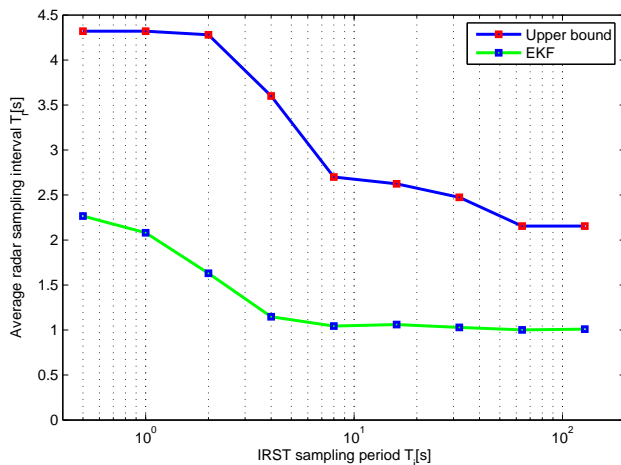


Figure 7: Average radar update time (in seconds) versus the IRST sampling period T_i ; blue line is the theoretical (upper) bound, green line is the EKF result

the EKF achieved only about half of the upper bound on average radar update time. It may be possible to approach the bound using a better tracking filter, such as an IMM [7, 9] with a number of acceleration states.

Note that the results do not take into account the potential errors in associating the measurements to the track. If measurements were incorrectly associated, a decrease in the average radar update time, or equivalently an increase in radar resources, would be required to maintain the desired track error limit.

5 Conclusions

The paper presented a theoretical analysis of phased-array radar allocation requirements for tracking anti-ship missiles with an integrated radar/IRST surveillance system. The main tool in the analysis was the posterior Cramer-Rao lower error bound for target tracking, and therefore the obtained results for the average radar update time indicate only the upper bound. The presented analysis allows us to quantify the IRST benefits in the anti-ship missile defence, without a need for extensive Monte Carlo simulations. The analysis was carried out using simplified radar and IRST models, characterised by measurement accuracies and probabilities of detection. Future work will extend the analysis by (1) using more realistic sensor models and (2) calculating a more accurate PCRLB in cluttered environments, via the enumeration of the measurement sequences as in [16]. Finally it will be necessary to verify the theoretical results by comparison with the experimental data.

References

- [1] M. L. Hernandez, B. Ristic, and A. Farina. A performance bound for manoeuvring target tracking using best-fitted Gaussian distributions. In *Proc. 8th Int. Conf. Information Fusion (Fusion 2005)*, Philadelphia, USA, 2005.
- [2] S. R. Horman, R. A. Stapleton, K.C. Hepfer, R. M. Headley, and J. K. Stapleton. Interactive integration of passive infrared and radar horizon surveillance sensors to extend acquisition and firm track ranges. In *Proc. Multi-sensor multi-target data fusion, tracking and identification techniques for guidance and control applications*, pages 14–31, AGARD-AG-337, Oct. 1996.
- [3] J.-M. Missirian and L. Ducruet. IRST: a key system in modern warfare. In *Proc. SPIE*, volume 3061, pages 554–565, 1997.
- [4] S. Blackman and R. Popoli. *Design and Analysis of Modern Tracking Systems*. Artech House, 1999.
- [5] S. S. Blackman, R. J. Dempster, S. H. Roszkowski, D. M. Sasaki, and P. F. Singer. Improved tracking capability and efficient radar allocation through the fusion of radar and infrared search-and-track observations. *Opt. Eng.*, 39(5):1391–1398, May 2000.
- [6] D. Maltese. Naval air defence: Multiple model approach to the angular tracking and targeting of anti-ship missiles. In I. Kadar, editor, *Proc. SPIE*, volume 4380, pages 63–74, 2001.
- [7] Y. Bar-Shalom, X. R. Li, and T. Kirubarajan. *Estimation with Applications to Tracking and Navigation*. John Wiley & Sons, 2001.
- [8] A. Averbuch, S. Itzikowitz, and T. Kapon. Radar target tracking - Viterbi versus IMM. *IEEE Trans. Aerospace and Electronic Systems*, AES-27(3):550–563, May 1991.
- [9] X. R. Li. Engineer’s guide to variable-structure multiple-model estimation for tracking. In Y. Bar-Shalom and W. D. Blair, editors, *Multitarget-Multisensor Tracking: Applications and Advances*, volume III, chapter 10, pages 499–567. Artech House, 2000.
- [10] H. L. VanTrees. *Detection, Estimation and Modulation Theory (Part I)*. John Wiley & Sons, 1968.
- [11] P. Tichavsky, C. H. Muravchik, and A. Nehorai. Posterior Cramer-Rao bounds for discrete-time nonlinear filtering. *IEEE Trans. Signal Processing*, 46(5):1386–1396, May 1998.
- [12] X. Zhang and P. K. Willett. Cramer-Rao bounds for discrete-time linear filtering with measurement origin uncertainty. In *Proc. of the Workshop on Estimation, Tracking and Fusion: A tribute to Y. Bar-Shalom*, pages 546–561, Monterey, CA, USA, 2001.
- [13] M. L. Hernandez, A. D. Marrs, N. J. Gordon, S. Maskell, and C. M. Reed. Cramer-Rao bounds for non-linear filtering with measurement origin uncertainty. In *Proc. 5th Int. Conf. Information Fusion (Fusion 2002)*, pages 18–25, Annapolis, MD, USA, 2002.
- [14] A. Farina, B. Ristic, and L. Timmoneri. Cramer-Rao bound for nonlinear filtering with $P_d < 1$ and its application to target tracking. *IEEE Trans. Signal Processing*, 50(8):1916–1924, August 2002.
- [15] M. Hernandez, B. Ristic, A. Farina, and L. Timmoneri. Comparison of two Cramer-Rao bounds for non-linear filtering with $P_d < 1$. *IEEE Trans. Signal Processing*, 52(9):2361–2370, 2004.
- [16] M. Hernandez, A. Farina, and B. Ristic. A PCRLB for tracking in cluttered environments: A measurement sequence conditioning approach. *IEEE Trans. Aerospace and Electronics Systems*, 2006. (In press).

- [17] M. Hernandez, B. Ristic, and A. Farina. A performance bound for Markovian switching systems using best fitting Gaussian distributions. *IEEE Trans. Signal Processing*, 2005. (Submitted).
- [18] M. I. Skolnik. *Introduction to Radar Systems*. McGraw-Hill, 1980.